

# Procrustes Analysis for the Virtual Trial Assembly of large-size elements

E. Maset<sup>a,\*</sup>, L. Scalera<sup>a</sup>, D. Zonta<sup>b</sup>, I. M. Alba<sup>b</sup>, F. Crosilla<sup>a</sup>, A. Fusiello<sup>a</sup>

<sup>a</sup>*Polytechnic Department of Engineering and Architecture, University of Udine, Italy*

<sup>b</sup>*Cimolai S.p.A., Pordenone, Italy*

---

## Abstract

Virtual assembly is an essential method to increase efficiency and to identify potential issues of the assembly process in several manufacturing fields, as for instance robotized assembly. The paper presents a novel procedure based on *Affine Procrustes Analysis* for the Virtual Trial Assembly (VTA) of large-size elements. This approach to virtual assembly allows to identify possible discrepancies between the workpieces and their nominal specifications, and to automatically define shape and dimensions of the potential corrective elements needed to achieve the designed assembly. The method is a variation of the classical *Extended Orthogonal Procrustes Analysis* (a tool that provides the least squares alignment among corresponding points), and permits to easily verify the parallelism condition of planes of large-size elements and the satisfaction of the alignment tolerances in the components to be assembled. Furthermore, the method implicitly takes into account the presence of corrective elements, avoiding assembly errors propagation. Experiments show the feasibility of the proposed approach and its advantages with respect to the classical one. The novel method is applied to the challenging assembly of dogbones elements of Vessel in New York.

**Keywords:** Virtual Trial Assembly, Affine Orthogonal Procrustes Analysis, assembly analysis, computer-aided manufacturing, Vessel - New York

---

## 1. Introduction

Nowadays, assembly simulation is widely used in several manufacturing fields, from industrial robotics to complex installations, to increase the efficiency, verify the operations sequence, and identify potential issues of the assembly process [1]. This results in a reduction of product development cycles times and cost. Virtual assembly tools need to be flexible and reconfigurable, to rapidly adapt to product variability, and to cope with new requests from the markets. The main goals that a virtual assembly tool has to achieve include operations sequence scheduling [2], assembly planning [3, 4, 5], collision detection [6], and constraint recognition [7].

---

\*Corresponding author

Email address: [maset.eleonora@spes.uniud.it](mailto:maset.eleonora@spes.uniud.it) (E. Maset)

The assembly problem becomes more challenging when large-size steel elements, obtained with complex manufacturing processes, are taken into account. In this case, due to the performance of the manufacturing process, a residual between the size and shape of the workpiece and its technical specifications could emerge. Therefore, once the composing parts are manufactured, it is necessary to proceed with their technical control. This verification is carried out with different instruments according to the desired accuracy: metrology-grade laser trackers in the case of high precision measurements, topographic total stations otherwise.

In this context, a Virtual Trial Assembly (VTA) is required to verify the elements assemblability, since the compliance of the single pieces does not guarantee the assemblability of the whole product: small errors can accumulate in the assembly, resulting in an inadmissible deviation at some stage. Therefore, VTA is crucial in the computer-integrated manufacturing of complex structures, since it allows to analyze the discrepancies between the workpieces and their nominal parameters by a rigid transformation, and to simulate the assembly of as-built 3D models. If this process detects some issues, the VTA defines shape and dimensions of the corrective elements, which guarantee the complete assembly.

Once the VTA is carried out, the actual position of the elements during the assembly phases can be predicted by adding the nominal deformation values, computed through a Finite Element Method (FEM) model, to the coordinates computed by the VTA. This is a necessary step to compare the predicted positions with those subsequently measured on site, since the VTA does not consider the deformations to which the assembling elements are subjected.

The main contributions of this paper are the introduction of the *Affine Extended Orthogonal Procrustes Analysis* as an innovative strategy for the Virtual Trial Assembly of large-size elements, and the experimental validation of the method on an extremely challenging task, such as the assembly of the elements (the so-called *dogbones*) of *Vessel*. The proposed method, indicated as Affine-EOPA, is based on a variant of the *Extended Orthogonal Procrustes Analysis* (EOPA) [8], since it extends the space where EOPA can be applied from Euclidean (points) to affine (points and vectors). More in detail, the geometric conformity of each element is checked first by considering the parallelism of the manufactured flange planes w.r.t. the design values. After aligning the normals of the measured and nominal planes, the parallelism is verified by considering the residual angle between the actual and nominal normals. If the parallelism condition is satisfied, the procedure computes the robust translational components that align surveyed and design bolt hole coordinates. The algorithm is directly applied to assess the assemblability of the elements in compliance with the allowed tolerances. The proposed method is flexible and reconfigurable, and can be applied to the assembly of large-size elements in the fields of robotics, automation and innovative manufacturing systems.

The paper is organized as follows: Section 2 reviews several works on virtual assembly and its applications in the field of computer-integrated manufacturing. Section 3.1 recalls the concept of Procrustes Analysis, whereas in Section 3.2 the theory of the Affine-EOPA method is derived. Section 4 defines the VTA problem for the structure under study, and Section 5 illustrates the application of the proposed procedure to the case study. The experimental validation of the method and the results obtained with the proposed approach are presented in Section 6. Finally, Section 7 draws the conclusions of this work.

## 2. Virtual Assembly: State of the art

An emerging trend in manufacturing is represented by product proliferation, heterogeneous market, customization increase and shorter product life cycle [9]. Thus, the challenge that industries like manufacturing, automotive and construction are facing nowadays is to reduce production time and cost, in order to remain competitive in the marketplace. Virtual assembly and virtual prototyping are powerful tools to reach this goal, since visualizing and testing CAD models, before they are physically fabricated or during the early production stage, are effective ways to decrease product development cycle time [10]. In addition, virtual assembly systems could be used to identify and analyze problems that might arise during service and maintainability operations, and they could also provide a platform for the training of assembly workers [1].

In the last years, several computer-based tools to perform virtual assembly, which allow to map the real assembly operation process in a virtual environment, have been proposed in the literature. Exploiting virtual reality, real-time collision detection and assembly path planning can be achieved interactively.

The implementation of part positioning during an assembly can be obtained by means of two different methods: constraint-modeling and physics-based modeling [1]. The former approach uses inter-part geometric constraints (e.g., coplanarity of surfaces, alignment of rotation axes or tangency between adjacent parts) to determine relationships between components and to place the parts in their final position and orientation in the assembly. VADE (Virtual Assembly Design Environment) is one of the first developed constraint-based modeling systems for assembly motion simulation [11]. It consists of a virtual reality system, which allows to evaluate tolerance issues, select optimal component sequences, and generate assembly and disassembly process plans.

Yang et al. [7] integrated in IVAE (Integration Virtual Assembly Environment) algorithms for constraint recognition, constraint confirmation and motion navigation based on a degree-of-freedom analysis. The method proved to be efficient for a variety of products, including rotary crushers and automobile engines.

Another example is given by Liu and Tan [12], who presented a constrained manipulation approach that realizes assembly relationship recognition, constraint solution and constrained motion for interactive assembly in a virtual environment. Test cases confirm that, by applying this constraint-based approach, the efficiency of assembly relationship recognition is enhanced, and the assembly interaction facilitated. Nevertheless, possible interferences between components may be missed and no force feedback is provided in the virtual assembly.

Physics-based algorithms instead simulate friction, gravity as well as forces and torques acting on bodies in order to introduce a more realistic behavior in the assembly simulation [1]. In combination with haptic interfaces, physics-based methods allow users to touch and feel virtual models for a more intuitive interaction with the environment [13]. Gonzalez-Badillo et al. [14] proposed a new methodology to evaluate the performance of physics simulation engines used in haptic virtual assembly applications. Different parameters such as task completion time, influence of weight perception and force feedback are measured and compared. Furthermore, Yoon [15] presented an algorithm for the computation of optimal paths for haptic guidance and assembly sequence of the parts, showing good performance of the haptic guidance mode with respect to the unguided one.

An important technology to assist assembly operations, either in training and as an online guidance system, is augmented reality [16]. An example is given by Wang et al. [4], who presented a novel assembly simulation system incorporating real-virtual components interaction in an augmented-reality environment. A bare-hand interface is provided to enable users to manipulate virtual components, and resultant forces exerted on virtual objects from contacts with real components and manipulation of the user's hands are calculated.

Commonly, virtual assembly systems are based on CAD models of nominal size, however, it can also be implemented by using as-built models, such as laser-scanned ones. These can reflect the real surface features and the actual machining dimensions of the part, leading to a more realistic assembly simulation and a more accurate collision detection. For example, Yu et al. [17] proposed a virtual assembly method that exploits both geometric design and laser scanning to generate a repair scheme based on collision detection.

In complex multistage manufacturing systems, in addition to an accurate design of each step of the assembly, it is important to simulate and predict dimensional variation propagation as well. In [9] and [18], the stream-of-variation analysis (SOVA) is applied in the design phase to generate math-based prediction of potential individual assembly errors. These contribute to an accumulating set of dimensional variations, which can lead to parts and products out of tolerances. When applied in the production phase, instead, SOVA can be used to compare predicted misalignment with actual measurements to determine the degree of mismatch in the assembly and to isolate error sources. Other automatic techniques have been recently proposed for process monitoring, in order to identify variations that can occur during the production stage. For example, Pacella et al. [19] adopted a machine vision system and a non-parametric approach for statistical monitoring of free-form profiles.

When dealing with large-size elements, a trial assembly is required in order to verify the assemblability of 3D as-built models, satisfying the tolerances and the requirements of the project, as pointed out in [20, 21].

To the best of the authors' knowledge, in the literature only a few works can be found that apply the virtual assembly to as-built 3D models of large-size workpieces (see e.g. [22]).

Among them, Case et al. [23] proposed an algorithm based on Generalized Procrustes Analysis to perform the VTA of large-size steel structural elements. In that case, the global matching of all the manufactured elements was performed, starting from the measured data obtained by an accurate metric survey of the bolt holes locations of the fabricated pieces.

The aforementioned work demonstrates the usefulness of VTA and highlights how Procrustes Analysis can be a valuable tool to accomplish this task. For this reason, in the present paper Procrustes methods are further explored and a variation of the Extended Orthogonal Procrustes Analysis is proposed. The developed algorithm is experimentally validated performing the VTA of Vessel.

### 3. Theoretical framework

The term *Procrustes Analysis* refers to a set of least squares mathematical tools used to perform transformations among corresponding points belonging to a generic  $k$ -

dimensional space, in order to satisfy their maximum agreement. Procrustes Analysis is particularly appealing, since it does not need the knowledge of *a priori* unknown approximate parameter values and requires only matrices products and the Singular Value Decomposition of a  $k \times k$  matrix. Successfully applied in the last decades in many fields, e.g., multifactorial analysis [24], shape analysis [25], geodesy [26] and photogrammetry [27], these methods proved to be suited also to perform the VTA of a complex structure, as demonstrated in [23].

In this section we recall the theoretical framework of the classical Extended Orthogonal Procrustes Analysis and we highlight the shortcoming of this algorithm in the assembly problem of large-size elements. The limitations of the classical EOPA lead us to the development of a novel method, the Affine-EOPA, described in Section 3.2.

### 3.1. Classical Extended Orthogonal Procrustes Analysis

In the following we briefly review the well-known Extended Orthogonal Procrustes Analysis and derive the solving expressions for the similarity transformation between two point-sets; more details can be found in [28].

Given an origin matrix  $A$  and a destination matrix  $B$ , containing the coordinates of  $p$  points in  $\mathbb{R}^k$  by rows, the Extended Orthogonal Procrustes Analysis (EOPA) [8] allows to directly estimate the unknown similarity transformation, composed by the rotation matrix  $R$ , the translation vector  $\mathbf{t}$  and the global scale factor  $c$ , that minimizes the square of the Frobenius norm of the residual matrix  $E$ :

$$\|E\|_F^2 = \|B - cAR - \mathbf{1}\mathbf{t}^\top\|_F^2 \quad (1)$$

under the orthogonality condition  $R^\top R = RR^\top = I$ , with  $\mathbf{1} = [1_1, 1_2, \dots, 1_n]^\top$ .

This results in the cost function:

$$\begin{aligned} F &= \text{tr}(E^\top E) + \text{tr}[L(R^\top R - I)] \\ &= \text{tr}[B^\top B + c^2 R^\top A^\top AR + \mathbf{t}\mathbf{1}^\top \mathbf{1}\mathbf{t}^\top - 2cR^\top A^\top \mathbf{1}\mathbf{t}^\top - 2B^\top \mathbf{1}\mathbf{t}^\top - 2cB^\top AR + LR^\top R - L] \end{aligned} \quad (2)$$

where  $L$  is a diagonal matrix of Lagrangean multipliers. The minimization of (2) is achieved by setting to zero the derivative of the cost function with respect to the unknowns  $R$ ,  $\mathbf{t}$  and  $c$ :

$$\frac{\partial F}{\partial R} = 2c^2 A^\top AR - 2cA^\top B + 2cA^\top \mathbf{1}\mathbf{t}^\top + R(L + L^\top) = 0 \quad (3)$$

$$\frac{\partial F}{\partial \mathbf{t}} = 2\mathbf{1}^\top \mathbf{1}\mathbf{t} + 2cR^\top A^\top \mathbf{1} - 2B^\top \mathbf{1} = 0 \quad (4)$$

$$\frac{\partial F}{\partial c} = 2c \text{tr}(R^\top A^\top AR) - 2\text{tr}(R^\top A^\top B - R^\top A^\top \mathbf{1}\mathbf{t}^\top) = 0 \quad (5)$$

Please note that the product  $\mathbf{1}^\top \mathbf{1}$  generates a scalar  $p$ , corresponding to the number of rows of  $A$  and  $B$ . After multiplying Equation (3) on the left by  $R^\top$ , observing that  $R^\top A^\top AR$  and  $R^\top R(L + L^\top)$  are symmetric, one can notice that also

$$R^\top A^\top B - R^\top A^\top \mathbf{1}\mathbf{t}^\top \quad (6)$$

must be symmetric. Substituting in Equation (6) the expression of  $\mathbf{t}$  that results from (4):

$$\mathbf{t} = (B - cAR)^{\top} \frac{\mathbf{1}}{p} \quad (7)$$

the symmetric condition must be verified for the term:

$$R^{\top} A^{\top} B - R^{\top} A^{\top} \frac{\mathbf{1}\mathbf{1}^{\top}}{p} (B - cAR) = R^{\top} A^{\top} \left( I - \frac{\mathbf{1}\mathbf{1}^{\top}}{p} \right) B + cR^{\top} A^{\top} \left( \frac{\mathbf{1}\mathbf{1}^{\top}}{p} \right) AR. \quad (8)$$

Matrix  $J = \left( I - \frac{\mathbf{1}\mathbf{1}^{\top}}{p} \right)$  is symmetric and idempotent and its role is to translate the matrix values to which it is applied (in this case  $A$  and  $B$ ) to the corresponding barycenter. Noticing the symmetry of  $R^{\top} A^{\top} \left( \frac{\mathbf{1}\mathbf{1}^{\top}}{p} \right) AR$ , it consequently happens that:

$$R^{\top} A^{\top} JB \quad (9)$$

is also symmetric. Calling

$$S = A^{\top} JB, \quad (10)$$

it results:

$$R^{\top} S = (R^{\top} S)^{\top} = S^{\top} R \quad (11)$$

from which one can retrieve  $R$ :

$$R = UV^{\top} \quad (12)$$

with  $S = UD_sV^{\top}$  Singular Value Decomposition (SVD) of  $S$ . This equation only guarantees that  $R$  is orthogonal. The least squares estimate of a rotation matrix is obtained by [29]:

$$R = U \text{diag}(1, 1, \det(UV^{\top})) V^{\top}. \quad (13)$$

Once  $R$  is known, one can compute  $\mathbf{t}$  from (7) and the scale factor  $c$  from Equation (5). Substituting the expression for vector  $\mathbf{t}$ , the solution becomes:

$$c = \frac{\text{tr}[R^{\top} A^{\top} JB]}{\text{tr}[R^{\top} A^{\top} JAR]} = \frac{\text{tr}[R^{\top} A^{\top} JB]}{\text{tr}[A^{\top} JA]} \quad (14)$$

after having considered the orthogonality of  $R$ .

If the sought transformation is rigid, as it is the case in this work,  $c$  is dropped and set to one.

### 3.2. Affine-EOPA

Classical Procrustes Analysis operates only on sets of points, without taking into account the geometrical characteristics of a manufactured piece, such as the presence of planar surfaces. When performing the VTA of large-size elements, it seems appropriate to introduce the planarity constraints in the algorithm, in order to directly align the planes of the workpieces and to verify possibly also their parallelism.

Starting from this consideration, we can straightforwardly extend the space where the EOPA operates, the Euclidean one, to an *affine* space, where *points* and *vectors* are represented, each one by  $\mathbb{R}^k$ .

If matrix  $A$  is partitioned into points  $A_{pt}$  and vectors  $A_n$ , and  $B$  accordingly into  $B_{pt}$  and  $B_n$ , it is easy to see that the rotation is computed as usual (see Section 3.1) by:

$$R = U \operatorname{diag}(1, 1, \det(UV^\top)) V^\top \quad (15)$$

where  $S = UD_sV^\top$  is the SVD of

$$S = [A_{pt}J, A_n]^\top [B_{pt}J, B_n]. \quad (16)$$

Please note that  $J$  (whose effect is to translate the origin) is applied only to points and not to vectors, according to the affine interpretation. The translation vector instead depends only on points (not on vectors):

$$\mathbf{t} = (B_{pt} - cA_{pt}R)^\top \mathbf{1}/p. \quad (17)$$

This method will be henceforth dubbed *Affine Extended Orthogonal Procrustes Analysis* (Affine-EOPA).

In a VTA context, if we assume that the elements are represented by points (either deriving from the survey of the object or from a project model) and that we can partition the point set into planes (at least two), Affine-EOPA allows to directly align planes, defined through their normals.

Let us now assume that each plane can slide along its normal without this influencing the alignment result (the residual orthogonal distance between the planes can be easily filled by a plate of adequate thickness in the assembly process). In other words, the position of each plane is undetermined along its normal. To take this assumption into account, which will be better clarified in the case study, point coordinates shall be used in the Procrustes Analysis in such a way they do not pose any constraint on  $\mathbf{t}$  along the normal of the plane they belong to. The solution can be then constructed as follows:

1. Rotation is computed only from plane normals;
2. For each plane, Equation (17) for  $\mathbf{t}$  is projected onto the plane itself, therefore cancelling any component along the plane normal.

Hence, rotation is computed from the SVD of

$$S = A_n^\top B_n. \quad (18)$$

As for the translation, let us consider plane  $i$  and let  $\mathbf{n}_i$  be its normal. Moreover, let  $N_i = I - \mathbf{n}_i\mathbf{n}_i^\top$  be the projector onto the plane orthogonal to  $\mathbf{n}_i$ . By applying the projection to Equation (17) we get:

$$N_i \mathbf{t} = N_i (B_{pt}^i - A_{pt}^i R)^\top \mathbf{1}/p. \quad (19)$$

This is a system of three equations in the unknown  $\mathbf{t}$ . Since  $\operatorname{rank}(N_i) = 2$  by construction, only two are independent. With at least two planes we can stack enough independent equations and solve the resulting least squares system for  $\mathbf{t}$ .

In the remaining of this paper, we will refer to Affine-EOPA with undetermined motion components as *Slack Affine-EOPA*.

For a better comprehension of the proposed method, we now give a simple geometric interpretation of the searched solution. In the analyzed problem points belong to planes

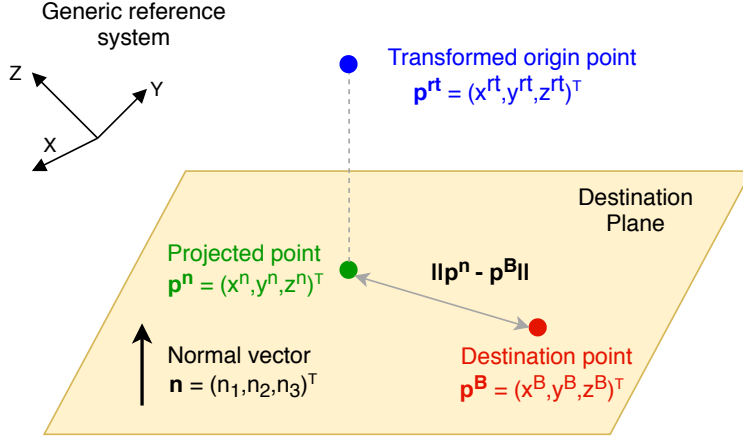


Figure 1: Minimization of the distance on the destination plane between destination and origin points.

and we want to minimize the distance between destination points and the projection of the origin points on the destination plane, previously rotated through matrix  $R$ . The situation is illustrated in Figure 1.

Let  $\mathbf{p}^A = (x^A, y^A, z^A)^\top$  and  $\mathbf{p}^B = (x^B, y^B, z^B)^\top$  be the origin and destination point, respectively. Let also  $\mathbf{p}^{rt} = (x^{rt}, y^{rt}, z^{rt})^\top$  be the transformed coordinates of the origin point, i.e.,

$$\mathbf{p}^{rt} = R^\top \mathbf{p}^A + \mathbf{t} \quad (20)$$

where  $\mathbf{t} = (t_x, t_y, t_z)^\top$  is the unknown translation vector and  $R$  is the rotation matrix computed with (15). Finally, let  $\mathbf{p}^n = (x^n, y^n, z^n)^\top$  be the projection of  $\mathbf{p}^{rt}$  onto the destination plane, defined by the following equation

$$n_1 x + n_2 y + n_3 z + s = 0 \quad (21)$$

with  $\mathbf{n} = (n_1, n_2, n_3)^\top$  normal vector,  $s = -(n_1 x^g + n_2 y^g + n_3 z^g)$  constant term and  $(x^g, y^g, z^g)$  coordinates of a generic point belonging to the plane. The distance to be minimized is therefore

$$d_{(\mathbf{p}^n, \mathbf{p}^B)} = \|\mathbf{p}^n - \mathbf{p}^B\|_2^2. \quad (22)$$

One can easily verify that the coordinates of the projected point  $\mathbf{p}^n$  can be expressed in the form

$$\mathbf{p}^n = N \mathbf{p}^{rt} - s \mathbf{n} \quad (23)$$

with the projector  $N$  depending only on the known nominal normal vector  $\mathbf{n}$ . Substituting (20) in (23), one obtains

$$\mathbf{p}^n = N \mathbf{t} + N R^\top \mathbf{p}^A - s \mathbf{n}. \quad (24)$$

The objective function to be minimized takes into account all the  $k_{pt}$  points belonging to each  $i$ -th plane. Assuming a total number of  $k_n$  planes, the cost can be written as

$$F(\mathbf{t}) = \sum_{i=1}^{k_n} \sum_{j=1}^{k_{pt}} \|(\mathbf{p}^n)_{i,j} - (\mathbf{p}^B)_{i,j}\|_2^2 = \sum_{i=1}^{k_n} \sum_{j=1}^{k_{pt}} \|N_i \mathbf{t} + N_i R^\top (\mathbf{p}^A)_{i,j} - s_i \mathbf{n}_i - (\mathbf{p}^B)_{i,j}\|_2^2 \quad (25)$$

where subscript  $j$  refers to the  $j$ -th point of plane  $i$ . The components of matrix  $N$  depend only from the destination planes, therefore a matrix  $N_i$  is defined for each plane. Setting to zero the derivatives of  $F(\mathbf{t})$  with respect to the unknowns  $(t_x, t_y, t_z)$ , the normal equations of system (19) can be obtained.

The proposed Slack Affine-EOPA method has been experimentally validated on a challenging case study: the assembly of dogbones elements of Vessel. The characteristics of the large-size elements that have to be assembled are described in the next section.

#### 4. Problem statement

Vessel is an installation located in the Hudson Yards district of New York [30]. To design Vessel, the architect, Thomas Heatherwick, found inspiration from the Indian water tanks, the so-called *pushkarani*, with a central small water lake at the bottom, reachable by a segmented staircase. The shape of Vessel is similar to a chalice or a vase (Figure 2), with a diameter at the base of almost 17 m, increasing to 40 m at the top. The total height is almost 46 m: it is possible to reach the top by walking along the stair ramps or by using an elevator that follows the structure profile. Vessel opened to the public on March 15, 2019.

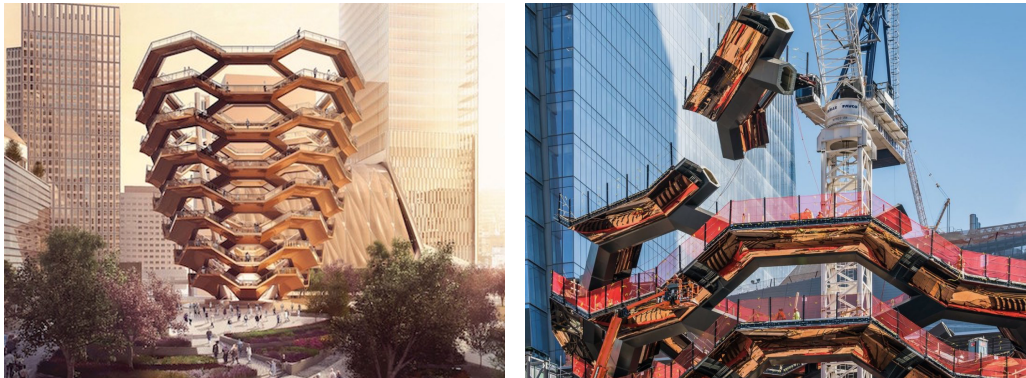


Figure 2: Rendering of Vessel and a construction phase (courtesy of Cimolai S.p.A.).

The most important elements of Vessel for the aims of this paper are the so called *dogbones*, built by the Italian company Cimolai S.p.A. They represent the steel units of the installation, and are connected to the neighbor ones by a series of four connection flanges per dogbone. The total number of dogbones is 65 (5 for each level, for a total of 13 levels) and the weight of each element is almost 25 t. Rising in elevation, the dimensions of the dogbones become wider, since the building diameter increases with height. Only the dogbones belonging to adjacent levels are connected; elements of the same level instead do not touch each other. In this way, every dogbone constitutes a landing to which four stair ramps are branched off, two upstairs and two downstairs.

The body of the dogbone (Figure 3) is constituted by a central gabion, to which four horns are successively welded. Staircases are welded in a second moment. A shim plate is located between the flanges of two adjacent dogbones, whose thickness can be modified in order to correct errors in the elements geometry, if necessary.

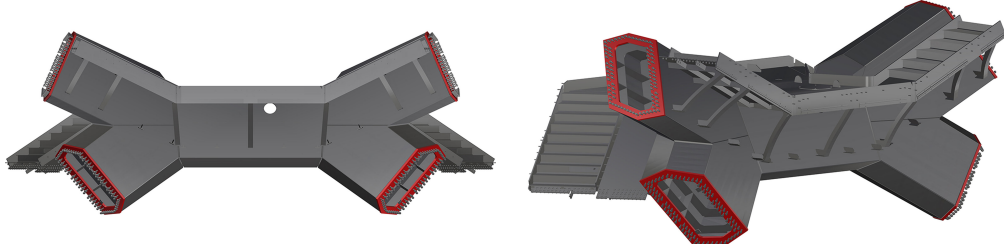


Figure 3: The large-size element of Vessel: the *dogbone* (courtesy of Cimolai S.p.A.).

The manufacturing of the dogbone starts with the parallel construction of the central body and of the horns. At this stage, the dogbones have not yet undergone mechanical processing such as milling and drilling. The flanges appear therefore without any hole and their surface is not leveled by machine tools. In this phase the geometric control is directly carried out by the carpenters with proper instruments, so as to verify the project tolerances of the elements. After this test, two horns of the same dogbone are joined one to each other. The topographic control begins when the core steel skeleton of the dogbone is enveloped by a cladding. It is indeed necessary to guarantee the expected tolerances not only along the dogbone-dogbone connections, but also along the dogbone-cladding connections, which should be lower than 10 mm. If this value is satisfied, it is possible to carry on with the welding process of the dogbone central core and the two pairs of horns and with a further topographic control that identifies possible deformations caused by the welding cooling.

Two different kinds of machining follow the welding step: first, the milling process of flanges and lateral planes of the structure, so as to satisfy a planarity error of less than 0.1 mm, then the boring of the flange plane. All the operations are managed by a machine tool, using a CAD/CAM technology. The geometric survey of a finished element is carried out by a metrology-grade laser tracker that can reach precision of the order of  $10^{-5}$  m. Each dogbone is surveyed from two stations, thus allowing to measure two flanges at a time. To reciprocally align the two surveys, some control points are located around the dogbone. In particular, the laser tracker measures:

- the plane of the flanges. About 50 points on the flange are measured and the interpolating plane is fitted. It is important to evaluate the planarity of the milled surface and its inclination w.r.t. the nominal one;
- the edges of the flange. Each edge is geometrically projected on the flange plane and deviations from the project geometry have to be compatible with the misalignment tolerance;
- the holes on the flange. The hole axes are represented by points that have to respect manufacturing tolerances. As for the edges, also these points are projected on the flange plane.

Eventually, the result of the topographic survey is constituted by a series of points and vectors belonging to the interpolated flange planes, by means of which adjacent dogbones

are assembled. This represents the 3D model to be used for the virtual assembly of the as-built elements.

EOPA, described in Section 3.1, could be used to compare the geometry of an actual workpiece to the project one. In this case, the origin and destination matrices contain the coordinates of the measured and nominal holes, respectively. Exploiting the EOPA solution with fixed unitary scale factor ( $c = 1$ ), the survey of the dogbone is therefore aligned to the nominal configuration via a roto-translation and the residuals represent the differences between real and project values. Similarly, for the VTA the origin matrix contains the surveyed points of the dogbone to be assembled, whereas the destination matrix is composed by the coordinates of the dogbones belonging to the lower level, virtually assembled in a previous step. Please note that, since dogbones of the same level are not directly connected and the assembly of an element depends only on the position assumed by the lower level ones, it is not necessary to consider together the configuration of several elements, i.e., it is not required to resort to the Generalized Procrustes Analysis, that simultaneously aligns multiple elements.

If directly applied to the case study, the classical EOPA method could produce misleading results. In fact, during the machining of the dogbone flanges, some of them can be milled with an offset of some millimeters in the orthogonal direction to the plane. This difference does not represent a problem for the assembly of the whole structure, because it can be easily filled by a shim plate. Nevertheless, ordinary EOPA does not take into account the possible offset and does not allow to reach the correct alignment between the survey and the project model, since it minimizes the 3D Euclidean distance between corresponding points. Figure 4 illustrates the problem and the result obtained by the direct application of the EOPA solution.

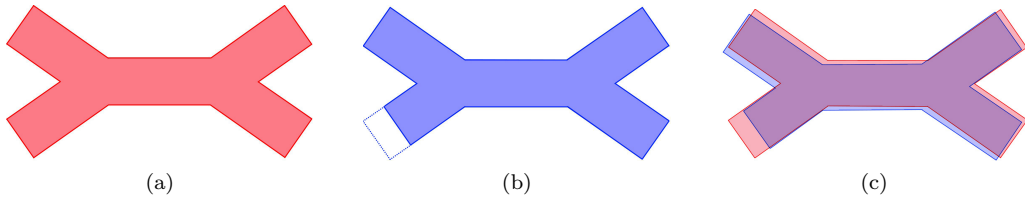


Figure 4: Problem connected to the EOPA approach. The red dogbone (a) represents the nominal configuration, the blue element is instead the measured one. Please note that the lower-left flange is machined with an offset that can be corrected with a customized shim plate. The desired alignment is shown in (b), whereas the ordinary EOPA solution achieves the solution shown in (c).

For this reason, rather than minimizing the distances between nominal and measured bolt holes, it is advisable to first search for the alignment of the flange planes, or, equivalently, to find the rotation that best aligns their normals. The alignment between the bolt holes should be determined in a subsequent step, through an estimate of the translation between the rotated configuration and the nominal one, that takes also into account that the position of the bolt holes does not pose any constraint along the normal of the plane they belong to. In this way, when performing the VTA of the structure, machining flaws could be easily identified and corrected by a shim plate, avoiding to compute incorrect rigid transformations that, propagating through the various levels, lead to a configuration far from the project values (see Figure 5).

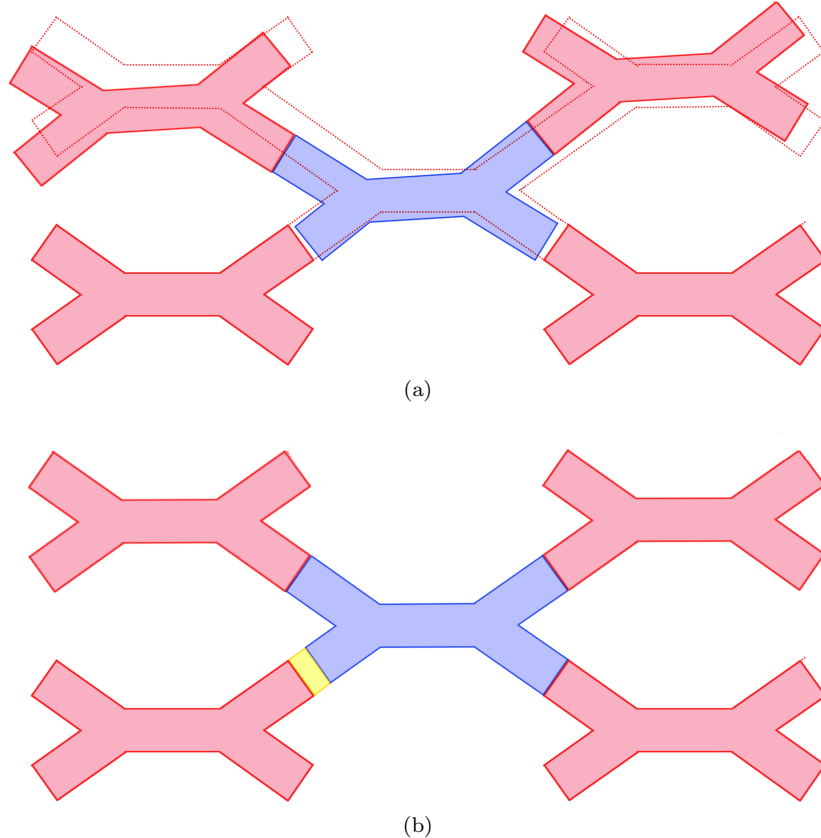


Figure 5: VTA performed by the ordinary EOPA solution (a) and desired result (b) that can be achieved by inserting a single shim plate (yellow rectangle).

It is easy to see that the solution sought is represented by our Slack Affine-EOPA algorithm. In the following we propose a procedure based on the method described in Section 3.2, that exploits the results of the survey to first verify the geometry of each element against the project values and then to perform the Virtual Trial Assembly. The VTA aims at understanding how possible defects of the dogbones belonging to the lower levels and discrepancies with respect to the nominal shape can influence the assembly of the upper level elements.

## 5. Case study: the assembly of dogbones elements of Vessel

Starting from the considerations made in the previous sections, we developed a robust assembly procedure based on Slack Affine-EOPA, that allows to:

- verify the actual geometry of each element to be assembled compared to the nominal one;

- perform the Virtual Trial Assembly of the whole structure, highlighting potential flaws that can prevent the structure to be assembled.

As shown in Figure 6, the proposed procedure is composed of two main steps. The goal of the first stage is to retrieve the rotation matrix  $R$  that allows to align the planes of the flanges surveyed with the laser tracker to the nominal configuration. The input data are the measured and nominal points corresponding to the center of the bolt holes. So, for each flange  $f_i$  ( $i = 1, \dots, 4$ ), the measured and nominal planes are estimated from the subset of  $k_{pt}$  points belonging to the  $i$ -th flange.

More in detail, the best fitting plane is estimated exploiting the Principal Component Analysis (PCA) [31] and the normal vector is computed as the eigenvector corresponding to the smallest eigenvalue of the covariance matrix built from the point coordinates. It is important to underline that, for each plane, two normals with the same direction but different orientation can be defined. In this case, the outward-pointing normal vectors are chosen.

Hence, origin matrix  $A_n$  and destination matrix  $B_n$  containing in each row measured and nominal normals, respectively, are used to estimate through Equations (15) and (18) the rotation  $R$  that maximizes in the least squares sense the parallelism of measured and nominal flange planes.

Residuals deriving from this transformation are correlated to the discrepancy in inclination between the manufactured flanges and the nominal ones. The angular difference  $\gamma_i$  between the rotated and nominal configuration of each flange  $i$  (described by the  $i$ -th row of matrix  $A_nR$  and  $B_n$ , respectively) can be computed as

$$\gamma_i = \arccos \frac{(A_n R)_{i,\cdot} \cdot (B_n)_{i,\cdot}^\top}{\|(A_n R)_{i,\cdot}\| \| (B_n)_{i,\cdot} \|} \quad (26)$$

and compared with the maximum allowed deviation  $\gamma_{max}$ , defined by the regulations. If the following condition

$$\gamma_i \leq \gamma_{max} \quad (27)$$

is not satisfied for all flanges, the rotational alignment is not correct and further analysis is needed. We assume that one over four flanges of the dogbone may have a wrong inclination, and a robust procedure is carried out to identify this outlying flange, whose inclination is far from the nominal value. More specifically, the rotation is calculated excluding one flange at a time from the input data, i.e., deleting one row from matrices  $A_n$  and  $B_n$  and verifying condition (27) at each iteration. This method allows to detect the possible outlier flange and at the same time to estimate a rotation matrix that is not biased by it. In this way, the rotated configuration of inlier flanges is perfectly aligned to the nominal geometry, while the inclination error of the outlier plane can be corrected during the assembly of the structure using, e.g., a wedge shim.

Once the rotation has been estimated, the final translation that aligns measured and nominal holes is computed as described in Section 3.2, solving the linear system (19). Thanks to this approach, if a flange presents an offset, it is successfully aligned to the nominal configuration, as shown in Figure 7.

After the application to the measured points of the roto-translation parameters estimated by the Slack Affine-EOPA solution, the residuals with respect to the nominal configuration can be studied. In particular, the components of the residual vector perpendicular to the nominal flange plane are used to adjust the thickness of the shim plate

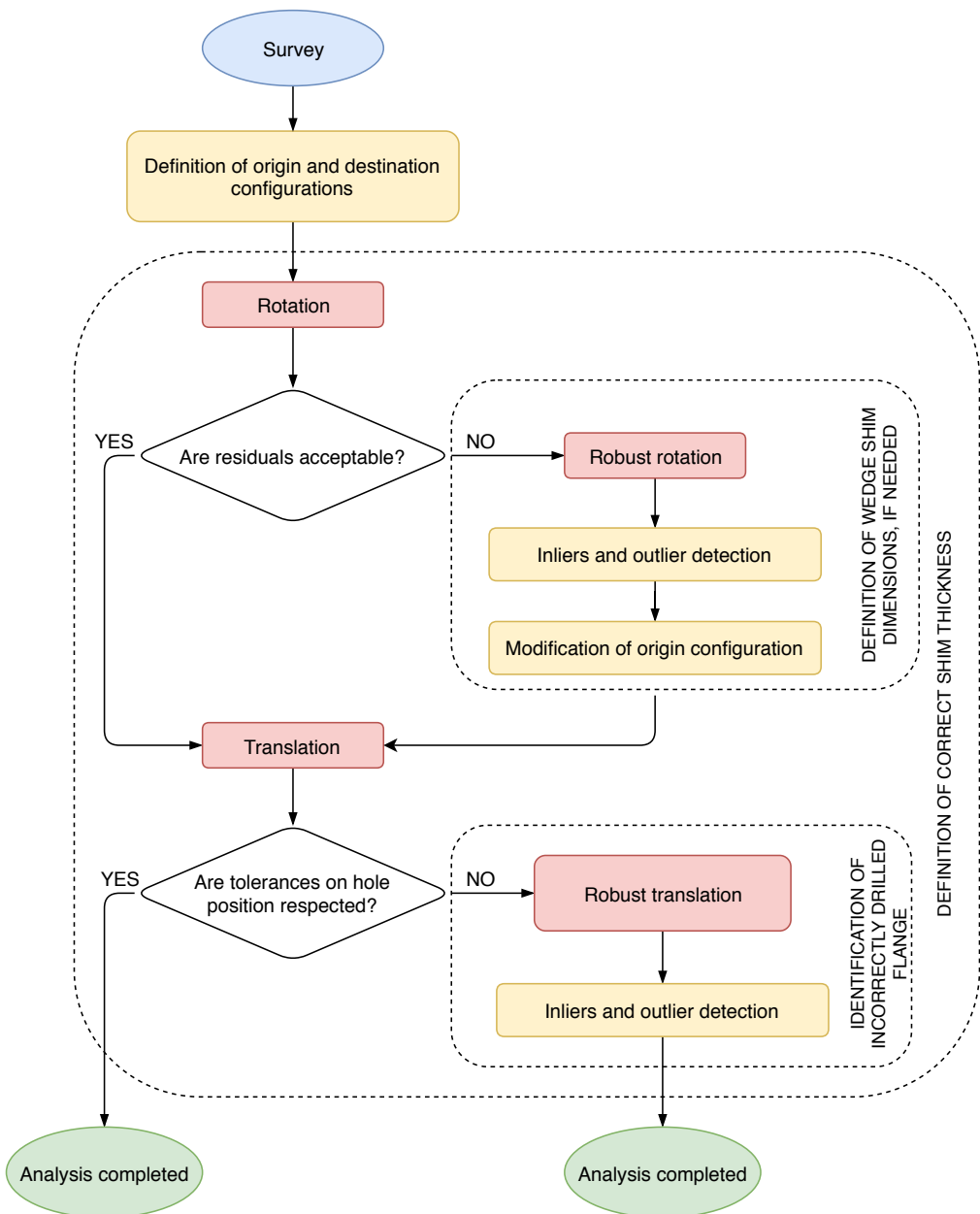


Figure 6: Flowchart of the proposed method.

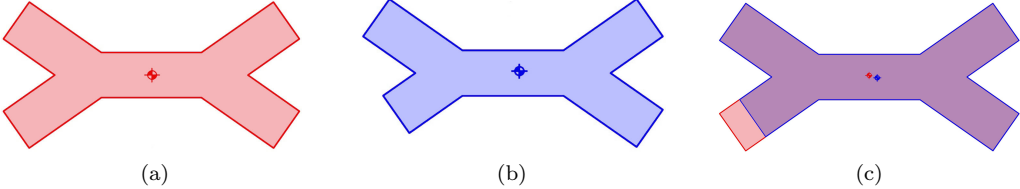


Figure 7: Project configuration (a), actual geometry (b) and alignment obtained via Slack Affine-EOPA (c).

placed between adjacent dogbones. The projection on the plane of the residual vector, instead, is compared to the tolerance imposed for the realization of the bolted connection. If the condition is not verified, a robust procedure is carried out, similarly to what is done to estimate a robust rotation matrix. More in detail, the computation is repeated considering three flanges at a time, in order to robustly compute  $\mathbf{t}$  and to localize the flange (one over four) that does not respect the tolerance.

To summarize, when applied to a single dogbone, the proposed procedure allows to check the geometry w.r.t. the nominal one, identifying possible outlier flanges, and permits to preliminary evaluate the correct thickness of the shims and the possibility to realize the bolted connections between adjacent dogbones.

As already mentioned, the developed algorithm can be applied with minor changes for further analysis on the assemblability of the whole structure. In fact, it can be used to perform the VTA of all the workpieces, verifying in this way not only the geometry of each single built dogbone, but also that they can be connected to each other, respecting the tolerances imposed by the regulations.

Since dogbones of the same level do not touch each other, each element can be analyzed independently. Going into detail, the VTA of a dogbone belonging to level  $n$  is achieved assuming in this case that the destination configuration is represented by the upper flanges of the dogbones belonging to level  $n - 1$ . The origin configuration, instead, is constituted by the two lower flanges of the dogbone to be assembled. Thus the roto-translation that best aligns a dogbone with the lower level ones is computed by the same algorithm previously presented, with the difference that in this situation only two flanges can be considered. For this reason, the robust analysis and the subsequent detection of the outlier flange that must be corrected is performed only during the comparison between actual and nominal geometry, as it requires four flanges. Figure 8 illustrates the VTA process. Red dogbones represent the elements already assembled, whereas the gray workpiece is the one under study.

As stated above, a shim plate is placed between adjacent dogbones. Its thickness has a default value of 25 mm, but it can be modified in order to compensate for the flaws generated by the machining. A first value of the thickness correction is computed in the previous step, i.e., when the geometry of each single dogbone is verified. However, a more accurate correction can be estimated during the VTA process, that allows to take into account also the geometry of lower level dogbones that influence the real assembly. The final thickness value is directly computed by the proposed procedure, analyzing the residual distance in the normal direction between a flange of level  $n$  and the corresponding one of level  $n - 1$  after the translation process. The VTA procedure allows therefore

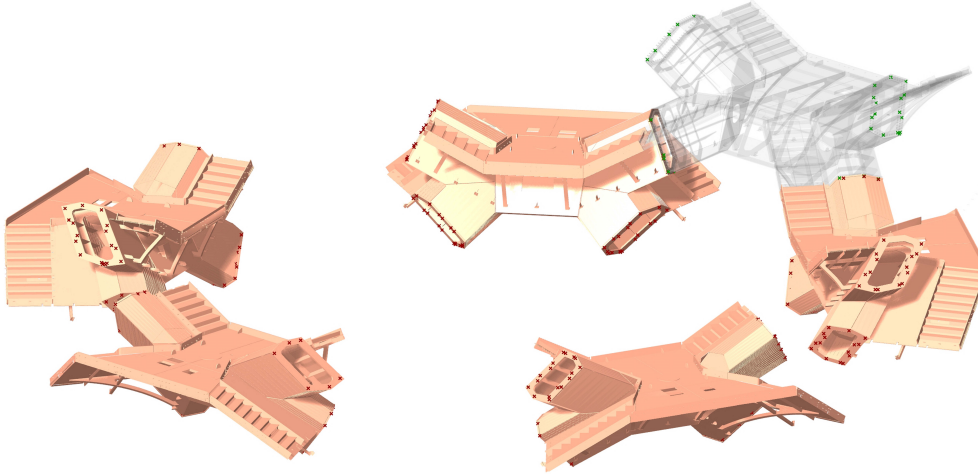


Figure 8: A step of the Virtual Trial Assembly process. Red dogbones represent the elements already assembled, whereas the gray workpiece is the one under study.

to estimate the most appropriate shim thickness between dogbones and to check the feasibility of the bolted connections in an efficient and automatic way.

## 6. Experimental results

The proposed method has been successfully applied to verify the geometry of the workpieces of Vessel and to perform the VTA of its levels. In the following, results of the comparison between surveyed and nominal geometry of a dogbone are reported in detail, together with the differences that arise when applying the ordinary EOPA method (with unitary scale factor) instead of the proposed Slack Affine-EOPA (shortened to SA-EOPA in the tables).

The element chosen as case study (dogbone 421 belonging to level 8) presents some flanges that were milled with an offset with respect to the nominal geometry. As previously illustrated, these flaws do not constitute a problem for the complete assembly, as they can be corrected through shims of adequate thickness. However, they can alter the results obtained by the EOPA.

Table 1 reports the distances on the nominal plane between roto-translated surveyed holes and nominal ones, i.e.,  $\|\mathbf{p}^n - \mathbf{p}^B\|$  (see Section 3.2). Discrepancies  $\Delta$  between the two tested approaches are shown as well. According to the developed procedure, differences between surveyed and nominal holes range from 0.07 mm to 0.48 mm. As clearly shown in Figure 9, that reports the boxplot of the residuals projected on the nominal plane, these values are much less than 1 mm, in compliance with the tolerances imposed by the regulations. The differences computed by EOPA, instead, vary between 0.03 mm and 1.94 mm. These results are biased by the flaws generated during the milling procedure, that negatively affect the roto-translation computed to align nominal

Hole	EOPA [mm]	SA-EOPA [mm]	$\Delta$ [mm]	Hole	EOPA [mm]	SA-EOPA [mm]	$\Delta$ [mm]
1.1	0.21	0.28	0.07	3.1	0.84	0.21	-0.63
1.2	0.36	0.20	-0.16	3.2	1.20	0.26	-0.94
1.3	0.22	0.48	0.26	3.3	1.29	0.41	-0.88
1.4	0.29	0.37	0.08	3.4	1.35	0.30	-1.05
1.5	0.26	0.45	0.19	3.5	1.43	0.32	-1.11
1.6	0.53	0.38	-0.15	3.6	1.40	0.20	-1.20
1.7	0.91	0.22	-0.69	3.7	1.52	0.31	-1.21
1.8	0.68	0.19	-0.49	3.8	1.47	0.28	-1.19
1.9	0.69	0.18	-0.51	3.9	1.54	0.16	-1.38
1.10	0.73	0.37	-0.36	3.10	1.54	0.19	-1.35
1.11	0.63	0.30	-0.33	3.11	1.35	0.08	-1.27
1.12	0.54	0.15	-0.39	3.12	1.41	0.21	-1.20
1.13	0.47	0.22	-0.25	3.13	1.33	0.14	-1.19
1.14	0.44	0.19	-0.25	3.14	1.18	0.32	-0.86
1.15	0.40	0.33	-0.07	3.15	1.09	0.32	-0.77
1.16	0.23	0.23	0.00	3.16	1.04	0.24	-0.80
1.17	0.22	0.22	0.00	3.17	1.06	0.21	-0.85
				3.18	0.91	0.14	-0.77
2.1	1.42	0.27	-1.15	4.1	0.67	0.47	-0.20
2.2	1.48	0.09	-1.39	4.2	0.33	0.33	0.00
2.3	1.32	0.26	-1.06	4.3	0.03	0.34	0.31
2.4	1.81	0.21	-1.60	4.4	0.20	0.22	0.02
2.5	1.79	0.07	-1.72	4.5	0.74	0.48	-0.26
2.6	1.78	0.15	-1.63	4.6	0.43	0.18	-0.25
2.7	1.76	0.17	-1.59	4.7	0.46	0.24	-0.22
2.8	1.81	0.11	-1.70	4.8	0.60	0.14	-0.46
2.9	1.94	0.27	-1.67	4.9	0.71	0.19	-0.52
2.10	1.62	0.23	-1.39	4.10	0.79	0.20	-0.59
2.11	1.22	0.38	-0.84	4.11	0.69	0.08	-0.61
2.12	1.16	0.32	-0.84	4.12	0.55	0.27	-0.28
2.13	1.33	0.16	-1.17	4.13	0.49	0.20	-0.29
2.14	1.19	0.27	-0.92	4.14	0.59	0.23	-0.36
2.15	1.29	0.12	-1.17	4.15	0.38	0.20	-0.18
2.16	1.21	0.17	-1.04	4.16	0.55	0.28	-0.27
				4.17	0.64	0.26	-0.38

Table 1: Comparison between residuals projected on the nominal plane obtained through EOPA and Slack Affine-EOPA.

Flange	EOPA			SA-EOPA		
	Max [mm]	Min [mm]	Average [mm]	Max [mm]	Min [mm]	Average [mm]
1	0.91	0.21	0.46	0.48	0.15	0.28
2	1.94	1.16	1.51	0.38	0.07	0.20
3	1.54	0.84	1.28	0.41	0.08	0.24
4	0.79	0.03	0.52	0.48	0.08	0.25

Table 2: Summary values of the residuals projected on the nominal plane obtained through EOPA and Slack Affine-EOPA.

and surveyed bolt holes. Summary statistics for each flange are reported in Table 2. Average residuals deriving from Slack Affine-EOPA are negligible, being less than 0.30 mm, whereas average residuals computed by the ordinary EOPA solution are greater than 1 mm for Flange 2 and 3 (1.51 mm and 1.28 mm, respectively). This could lead to the erroneous conclusion that two flanges can not be bolted.

It is interesting to evaluate also the residuals in the normal direction of the nominal

Flange	EOPA			SA-EOPA		
	Max [mm]	Min [mm]	Range [mm]	Max [mm]	Min [mm]	Range [mm]
1	+2.44	+1.12	1.32	+3.82	+2.87	0.95
2	+2.26	+1.60	0.66	+1.70	+1.12	0.58
3	-0.19	-0.42	0.23	+0.22	-0.08	0.30
4	-1.58	-1.89	0.31	-3.23	-3.66	0.43

Table 3: Comparison between residuals in the normal direction of the nominal plane obtained through EOPA and Slack Affine-EOPA.

		EOPA		SA-EOPA	
		Shim thick. [mm]	Residual [mm]	Shim thick. [mm]	Residual [mm]
Dogbone 405	Flange 1	24.8	0.5	25.9	0.6
	Flange 2	24.9	0.4	21.2	0.4
Dogbone 406	Flange 1	24.5	0.6	26.4	0.5
	Flange 2	24.6	0.7	21.7	0.6
Dogbone 407	Flange 1	25.4	1.9	25.9	0.4
	Flange 2	23.2	1.8	22.4	0.8
Dogbone 408	Flange 1	25.1	1.8	23.2	1.0
	Flange 2	26.0	1.2	28.1	1.4
Dogbone 409	Flange 1	23.7	0.9	21.9	1.5
	Flange 2	24.4	1.1	24.3	0.9

Table 4: Results of the VTA process. Shim thickness and the average residual projected on the flange plane are reported.

plane (Table 3). For each flange, the maximum and minimum residual values and their absolute difference are reported. The latter is a measure of the discrepancy in inclination between the built flange and the nominal one. If it is low (e.g., less than 1 mm), the lack of parallelism is negligible and no customized wedge shim is needed. For the dogbone under study, one can notice that Flange 1 presents a higher deviation; nevertheless, the discrepancy computed with the proposed approach is acceptable (0.95 mm) and no further robust analysis is required. Different considerations can be done when the surveyed and the nominal configurations are aligned through the classical EOPA. In this case, Flange 1 shows a significant discrepancy in inclination between the as-built plane and the project one, which would require a wedge shim. The mean value of the residuals along the normal direction can be taken as an approximate correction of the shim thickness, that can be refined during the subsequent VTA process. It is important to underline that higher residuals along the normal direction do not mean worse results, since in this case they only represent the shim correction needed and do not affect the assemblability. Lower residual values generated by the EOPA method for Flanges 1 and 4 with respect to Slack Affine-EOPA (Table 3) derive from the different roto-translation applied, that changes the residual distribution in the 3D space.

As already mentioned, the proposed method has been applied with minor changes to simulate the assembly of the structure, allowing to identify any critical issue that may arise during the assembly phases on site. Specifically, we assume as starting point the position of the dogbones belonging to level 4. The surveyed dogbones of this level are individually roto-translated with respect to their nominal configuration and represent the destination configuration of the elements belonging to level 5. Dogbones of the upper

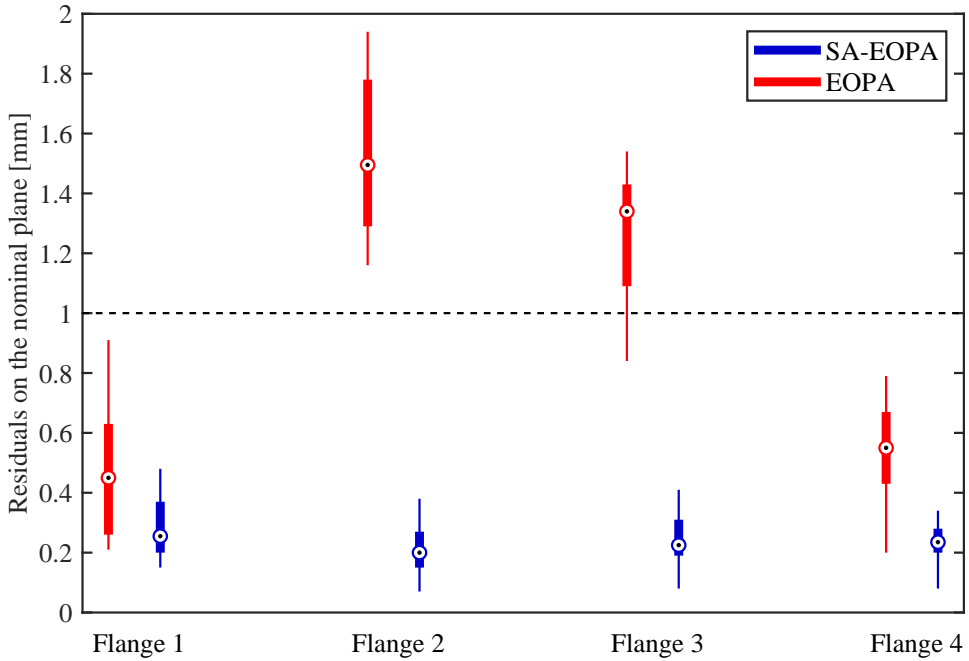


Figure 9: Boxplot of the residuals projected on the nominal plane between surveyed and nominal holes. The horizontal dashed line represents the tolerance value imposed by the regulations.

levels are then virtually assembled following the procedure described in Section 5, i.e., the lower flanges of each dogbone of level  $n$  are aligned with the upper flanges of the workpieces of level  $n - 1$ .

Results obtained for the VTA of dogbones belonging to level 5 are reported in Table 4. The VTA process highlights another advantage of the Slack Affine-EOPA compared to the EOPA. In fact, the developed algorithm implicitly takes into account the presence of the shims and the VTA of an element can be performed directly, without any modification of the hole coordinates. EOPA, instead, requires the preliminary adjustment of the destination configuration: points on the dogbone flanges of the lower level must be translated along the normal direction of 25 mm, that is the nominal shim thickness. Without this preprocessing step, EOPA, that aims at minimizing the 3D distance between corresponding points, tends to “squash” the dogbones of the upper level on those of the lower level. Results of the ordinary EOPA reported in Table 4 are obtained after the application of the aforementioned correction to the destination configuration.

The validity of the proposed method was confirmed during the physical assembly. In fact, the results of the VTA were compared with the surveys carried out on site, showing a tight correspondence between what was predicted by the VTA and the physical realization. Moreover, the absence of problems for the dogbones installation demonstrated the correctness of the values chosen for the shim thickness, calculated through the procedure described in Section 5.

## 7. Conclusions

Virtual Trial Assembly is a powerful tool to simulate the assembly process and to verify both the single connections and the final geometry in the assembly of large-size elements. Indeed, before the physical assembly, it is often necessary to verify the geometric congruence of the manufactured elements with respect to the project values and the assemblability of the workpieces, in compliance with the tolerances imposed by the regulations.

In this paper we proposed the introduction of the Affine Extended Orthogonal Procrustes Analysis as an innovative strategy for the VTA of large-size elements, and the experimental validation of the method on the assembly of the dogbones of the Vessel in Hudson Yards, New York. The developed algorithm allows to automatically verify the geometry of the manufactured complex elements and to perform the Virtual Trial Assembly of the whole realization, taking into account the geometrical characteristics of the workpieces. The method, in fact, is thought to maximize the parallelism of the planes belonging to adjacent elements and to optimize the possibility to realize the bolted connections between them. In particular, within the VTA it is possible to define shape and dimensions of the corrective elements, by means of which the complete assembly can be correctly achieved.

Experimental results on the challenging assembly of Vessel show the feasibility of the proposed approach and its advantages with respect to the classical method previously applied.

The presented method for the VTA of complex steel elements is flexible and reconfigurable, and it is proven to be an useful framework to verify the assembly of as-built 3D models. In future work, the proposed approach can be applied to successfully perform the virtual assembly of large-size elements in the fields of industrial automation and innovative manufacturing systems.

## Funding Source Declaration

This research did not receive any specific grant from funding agencies in the public, commercial, or not-for-profit sectors.

Declarations of interest: none.

## References

- [1] A. Seth, J. M. Vance, J. H. Oliver, Virtual reality for assembly methods prototyping: a review, *Virtual reality* 15 (1) (2011) 5–20.
- [2] F. Demoly, A. Matsokis, D. Kiritsis, A mereotopological product relationship description approach for assembly oriented design, *Robotics and Computer-Integrated Manufacturing* 28 (6) (2012) 681–693.
- [3] N. Ye, P. Banerjee, A. Banerjee, F. Dech, A comparative study of assembly planning in traditional and virtual environments, *IEEE Transactions on Systems, Man, and Cybernetics, Part C (Applications and Reviews)* 29 (4) (1999) 546–555.
- [4] X. Wang, S. Ong, A. Nee, Real-virtual components interaction for assembly simulation and planning, *Robotics and Computer-Integrated Manufacturing* 41 (2016) 102–114.
- [5] G.-C. Vosniakos, J. Deville, E. Matsas, On immersive virtual environments for assessing human-driven assembly of large mechanical parts, *Procedia Manufacturing* 11 (2017) 1263–1270.

- [6] G. Chryssolouris, D. Mavrikios, D. Fragos, V. Karabatsou, A virtual reality-based experimentation environment for the verification of human-related factors in assembly processes, *Robotics and Computer-Integrated Manufacturing* 16 (4) (2000) 267–276.
- [7] R. D. Yang, , X. Fan, D. Wu, J. Yan, Virtual assembly technologies based on constraint and dof analysis, *Robotics and Computer-Integrated Manufacturing* 23 (4) (2007) 447–456.
- [8] P. Schönemann, R. Carroll, Fitting one matrix to another under choice of a central dilation and a rigid motion, *Psychometrika* 35 (2) (1970) 245–255.
- [9] D. Ceglarek, W. Huang, S. Zhou, Y. Ding, R. Kumar, Y. Zhou, Time-based competition in multistage manufacturing: Stream-of-variation analysis (sova) methodology, *International Journal of Flexible Manufacturing Systems* 16 (1) (2004) 11–44.
- [10] C. Mascle, Feature-based assembly model for integration in computer-aided assembly, *Robotics and Computer-Integrated Manufacturing* 18 (5-6) (2002) 373–378.
- [11] S. Jayaram, H. I. Connacher, K. W. Lyons, Virtual assembly using virtual reality techniques, *Computer-aided design* 29 (8) (1997) 575–584.
- [12] Z. Liu, J. Tan, Constrained behavior manipulation for interactive assembly in a virtual environment, *The International Journal of Advanced Manufacturing Technology* 32 (7-8) (2007) 797–810.
- [13] A. Seth, H. J. Su, J. M. Vance, Sharp: a system for haptic assembly and realistic prototyping, in: ASME 2006 International Design Engineering Technical Conferences and Computers and Information in Engineering Conference, American Society of Mechanical Engineers, 2006, pp. 905–912.
- [14] G. Gonzalez-Badillo, H. I. Medellin-Castillo, T. Lim, J. M. Ritchie, R. CW Sung, S. Garbaya, A new methodology to evaluate the performance of physics simulation engines in haptic virtual assembly, *Assembly Automation* 34 (2) (2014) 128–140.
- [15] J. Yoon, Assembly simulations in virtual environments with optimized haptic path and sequence, *Robotics and Computer-Integrated Manufacturing* 27 (2) (2011) 306–317.
- [16] T. Masood, J. Egger, Augmented reality in support of industry 4.0 implementation challenges and success factors, *Robotics and Computer-Integrated Manufacturing* 58 (2019) 181–195.
- [17] A. Yu, Z. Liu, G. Duan, J. Tan, L. Che, X. Chen, Geometric design model and object scanning mode based virtual assembly and repair analysis, *Procedia CIRP* 44 (2016) 144–150.
- [18] W. Huang, Z. Kong, Simulation and integration of geometric and rigid body kinematics errors for assembly variation analysis, *Journal of manufacturing systems* 27 (1) (2008) 36–44.
- [19] M. Pacella, A. Grieco, M. Blaco, Machine vision based quality control of free-form profiles in automatic cutting processes, *Computers & Industrial Engineering* 109 (2017) 221–232.
- [20] J. C. Yuan, The control of fabrication and pre-assembly's dimension of tubular chimney tower, *Progress in Steel Building Structures* 3 (2011) 56–63.
- [21] Z. Yubin, Y. Jian, X. Youwu, Z. Yuling, Research and application of collision detection on steel structure in virtual pre-assembly environment, in: IOP Conference Series: Earth and Environmental Science, Vol. 199/3, IOP Publishing, 2018, p. 032046.
- [22] H. Zhang, D. Han, Y. Zhou, Z. Ren, X. Zhang, C. Dai, X. Wu, C. Hou, Virtual trial assembly of high-rise air corridor using bim and terrestrial laser scanning, in: 18th International Conference on Construction Applications of Virtual Reality, 2018, p. 556.
- [23] F. Case, A. Beinat, F. Crosilla, I. Alba, Virtual trial assembly of a complex steel structure by generalized procrustes analysis techniques, *Automation in Construction* 37 (2014) 155–165.
- [24] B. F. Green, The orthogonal approximation of an oblique structure in factor analysis, *Psychometrika* 17 (4) (1952) 429–440.
- [25] F. L. Bookstein, Size and shape spaces for landmark data in two dimensions, *Statistical Science* 1 (2) (1986) 181–222.
- [26] F. Crosilla, Procrustes analysis and geodetic sciences, in: Quo vadis geodesia...?, Vol. 1, Department of Geodesy and GeoInformatics, University of Stuttgart, 1999, pp. 69–78.
- [27] F. Crosilla, E. Maset, A. Fusielo, Procrustean photogrammetry: from exterior orientation to bundle adjustment, in: New Advanced GNSS and 3D Spatial Techniques, Springer, 2018, pp. 157–165.
- [28] J. C. Gower, G. B. Dijksterhuis, Procrustes problems, Oxford Statistical Science Series, Oxford University Press, 2004.
- [29] G. Wahba, A Least Squares Estimate of Satellite Attitude, *SIAM Review* 7 (3).
- [30] J. Fell, In numbers: Hudson Yards-Vessel, *Engineering & Technology* 11 (10) (2016) 16–17.
- [31] I. T. Jolliffe, Principal Component Analysis, Springer-Verlag, 1986.